Journal of Crystal Growth 475 (2017) 334–340

Contents lists available at ScienceDirect

Journal of Crystal Growth

journal homepage: www.elsevier.com/locate/crys

Crystal structure and composition of BAlN thin films: Effect of boron concentration in the gas flow

Shuo Wang [a], Xiaohang Li [b,c], Alec M. Fischer [a], Theeradetch Detchprohm [c], Russell D. Dupuis [c], Fernando A. Ponce [a,*]

[a] Department of Physics, Arizona State University, Tempe, AZ 85287-1504, USA
[b] King Abdullah University of Science and Technology (KAUST), Advanced Semiconductor Laboratory, Thuwal 23955-6900, Saudi Arabia
[c] Center for Compound Semiconductors and School of Electrical and Computer Engineering, Georgia Institute of Technology, Atlanta, GA 30332, USA

ARTICLE INFO

Article history:
Received 28 March 2017
Received in revised form 27 June 2017
Accepted 18 July 2017
Available online 20 July 2017
Communicated by T.F. Kuech

Keywords:
A1. Characterization
A1. Crystal structure
A3. Metalorganic chemical vapor deposition
B1. Nitrides
B2. Semiconducting III–V materials

ABSTRACT

We have investigated the microstructure of $B_xAl_{1-x}N$ films grown by flow-modulated epitaxy at 1010 °C, with B/(B + Al) gas-flow ratios ranging from 0.06 to 0.18. The boron content obtained from X-ray diffraction (XRD) patterns ranges from x = 0.02 to 0.09. On the other hand, boron content deduced from the aluminum signal in the Rutherford backscattering spectra (RBS) ranges from x = 0.06 to 0.16, closely following the gas-flow ratios. Transmission electron microscopy indicates the sole presence of a wurtzite crystal structure in the BAlN films, and a tendency towards columnar growth for B/(B + Al) gas-flow ratios below 0.12. For higher ratios, the BAlN films exhibit a tendency towards twin formation and finer microstructure. Electron energy loss spectroscopy has been used to profile spatial variations in the composition of the films. The RBS data suggest that the incorporation of B is highly efficient for our growth method, while the XRD data indicate that the epitaxial growth may be limited by a solubility limit in the crystal phase at about 9%, for the range of B/(B + Al) gas-flow ratios that we have studied, which is significantly higher than previously thought.

1. Introduction

The BAlGaN compound semiconductors (B-III-N) are being evaluated as a new alloy system for the next generation of photonic and electronic devices. Incorporating boron into the AlGaN system provides possibilities to further optimize the band gap energy and the lattice parameter, independently of each other, in order to minimize the effects of lattice mismatch. Examples of applications are as follows: BGaN can be lattice-matched to AlN and to SiC substrates [1]. BGaN micro-islands have been used as substrate for GaN overgrowth in order to achieve a low threading dislocation density [2]. High reflectivity deep-ultraviolet distributed Bragg reflectors (DBRs) based on BAlN materials can potentially surpass the performance of conventional AlGaInN DBRs in vertical-cavity surface-emitting lasers [3]. And BGaN thin layers have been introduced in AlGaN/GaN high electron mobility transistors to provide an electrostatic barrier to electrons and to improve the confinement of the 2-dimensional electron gas [4].

Previous reports indicate that it is difficult to obtain high quality B-III-N alloys over a broad range of B compositions while maintaining good crystallinity and smooth morphology [5–8]. Thermodynamic analysis for $B_xGa_{1-x}N$ and $B_xAl_{1-x}N$, typically grown by metalorganic chemical vapor deposition (MOCVD) at ~1000 °C, gives a high interaction parameter that is indicative of instability over most of the composition range of the alloy, with a reported B solubility limit of x = 0.018 and 0.028 in single-phase BGaN and BAlN, respectively [9]. Columnar growth has been observed in BAlN, with lateral dimensions of the order of 10 nm [10,11]. The difficulty in incorporating B may be associated with the high growth temperatures employed to enhance the surface migration of precursors and the production of undesirable adducts through gas-phase parasitic reactions between NH_3 and triethylboron [10].

Flow-modulated epitaxy (FME) is a useful method of producing III-V semiconductors, where the supply of group-III and group-V sources are injected alternately into the growth chamber without interruption [12]. In a layer-by-layer growth mechanism, FME causes complete surface coverage of the group-V atoms, thus increasing the diffusion length of group-III atoms. The intermittent supply of III vs V elements suppresses parasitic reactions in the gas

* Corresponding author.
E-mail address: ponce@asu.edu (F.A. Ponce).

http://dx.doi.org/10.1016/j.jcrysgro.2017.07.013
0022-0248/

phase, thus enhancing the metal incorporation in the film. We reported recently on the growth at 910 °C and 1010 °C of 100-nm thick single-phase wurtzite BAlN with boron content over 10% [13].

We present here the results of a systematic study of the boron content and microstructure of $B_xAl_{1-x}N$ films grown by FME at 1010 °C with B/III gas-flow ratios varying from 0.06 to 0.18. X-ray diffraction (XRD) analyses provide B contents that range from x = 0.026 to 0.085, whereas Rutherford backscattering spectrometry (RBS) provide boron contents close to the corresponding B/III gas-flow ratios. This discrepancy is explained by taking into consideration the microstructure and the spatial variation of the composition, which are obtained using transmission electron microscopy (TEM) and electron energy loss spectroscopy (EELS).

2. Experimental

The BAlN films were grown on *c*-plane AlN/sapphire templates at 1010 °C in a Close Coupled Showerhead 3 × 2″ Aixtron vertical reactor by FME using the *valves on/off* method. The Al, B, and N precursors were trimethylaluminum, triethylboron, and NH_3. In order to mitigate parasitic reactions in the vapor phase, we have used a low V/III ratio of 60. The study reported here is based on BAlN films grown with B/III gas-flow ratios of 0.06, 0.12, 0.15, and 0.18. All other growth parameters were the same for these films.

The boron content was estimated by XRD using Cu Kα (λ = 0.15406 nm) radiation and a four-crystal monochromator (4 × Ge (2 2 0)). The XRD area probed was 1 cm × 1 cm, limited by the mask on the X-ray source. The (0002) BAlN diffraction peak is related to the basal plane separation and is correlated to the boron content by Vegard's law (using c = 0.498 nm for AlN and c = 0.4213 nm for BN) [14]. In addition, the BAlN alloy composition was also estimated by RBS using a 2 MeV He^{++} ion beam, from an area probe of ~1.5 mm in diameter. The typical depth probe is about 1.5 μm. The detection sensitivity in RBS is poor for low-atomic-number elements. For this reason, the B content was derived from the RBS measurement of the Al content in the film, under the assumption of stoichiometry between the group III and V elements.

Cross-sectional TEM samples were prepared by mechanical wedge-polishing and ion milling with an Ar+ beam with 4.0 keV energy. We used a Philips CM-200 instrument, operated at 200 keV. EELS mapping was performed on the BAlN film with the highest B/III gas-flow ratio of 0.18, using a NION UltraSTEM 100 instrument, operated at 100 keV.

3. Results

Our study focuses on the evolution of the microstructure with boron content as determined by the B/III gas-flow ratio. The microstructures of our films present a high density of structural defects that affect our ability to accurately measure the boron content.

3.1. Measuring the boron content by XRD and RBS

The surface morphology of the films were relatively smooth, with a RMS surface roughness of about 2 nm [13]. Fig. 1 and Table 1 summarize the boron content in the four films, estimated from measurements by XRD and RBS. Notice that the boron content measured by RBS is found to be larger than when measured by XRD. In XRD, the diffraction intensity is plotted along a $\theta/2\theta$ scan; the patterns corresponding to our films are shown in Fig. 2. The XRD patterns consist of two peaks, one is centered at 18.016° and corresponds to the (0002) AlN reflection, and the other is a broader peak centered at a slightly higher angle and corresponds

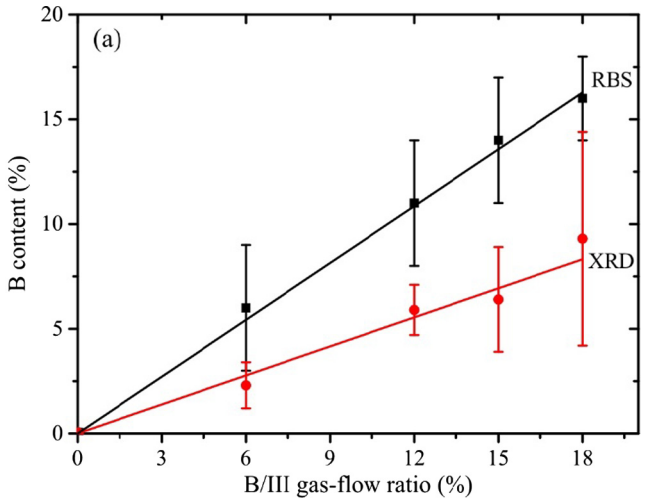

Fig. 1. Boron content in the film as a function of the B/III gas-flow ratio in the gas flow, determined by XRD (circles) and by RBS (squares), with corresponding linear fits.

Table 1
Boron content in the gas flow during growth, and in the thin film measured by XRD and RBS. Other growth parameters are kept constant: the growth temperature is 1010 °C, the V/III gas source ratio is 60, the TEB + TMA flow is 57 μmol/min, the growth rate is 0.32 nm/s. FME pulse period: TEB + TMA = NH_3 = 0.8 s. The film thickness is about 45 nm in all cases.

B/III	XRD		RBS		XRD/RBS
	[B]	Lattice Mismatch (%)	[B]	Lattice Mismatch (%)	
0.06	0.023	0.41	0.06	1.08	0.38
0.12	0.053	0.94	0.11	1.98	0.48
0.15	0.064	1.14	0.14	2.53	0.46
0.18	0.093	1.66	0.16	2.88	0.58

to the (0002) BAlN reflection. For example, the pattern for B/III = 0.12 presents a peak centered at 18.183° that correspond to a boron composition x = 0.059. The full-width-at-half-maximum (FWHM) of the BAlN peak is 0.11°. There are several ways to interpret the FWHM: (a) It is due to a boron composition variation; (b) it is due to defects and strain; and (c) it is due to particle-size broadening. The last one is most likely to be the case. The broadening due to film thickness can be estimated from Scherrer equation $B(2\theta) = \frac{K\lambda}{L\cos\theta}$ [15]. With $K \approx 1$, crystal size L = 45 nm, λ = 0.154 nm, the broadening is expected to be 0.0018 rad or 0.1° for θ near 18°, which is similar to the observed value of 0.11°.

The XRD intensity relies on Bragg diffraction from crystal planes that are parallel to the diffraction plane of the diffractometer, which is experimentally determined by alignment of the substrate. Therefore, regions in the BAlN film that are not parallel to the substrate will not contribute significantly to the measured XRD intensity in the $\theta/2\theta$ scan. Note that the BAlN peak is much weaker (3–5 orders of magnitude) than the AlN peak, making reciprocal space maps not very useful [13].

Composition determination by RBS is achieved by measuring the backscattering of a beam of alpha particles. The recoil energy of the backscattered particles depends on the atomic weight of the individual atomic constituent, according to an elastic collision where kinetic energy is conserved. The measured energy is also affected by the distance of the scattering atoms to the surface of the material, since some energy is dissipated by friction between the alpha particle and the material. In this manner, the RBS technique allows the measurement of the average composition as a

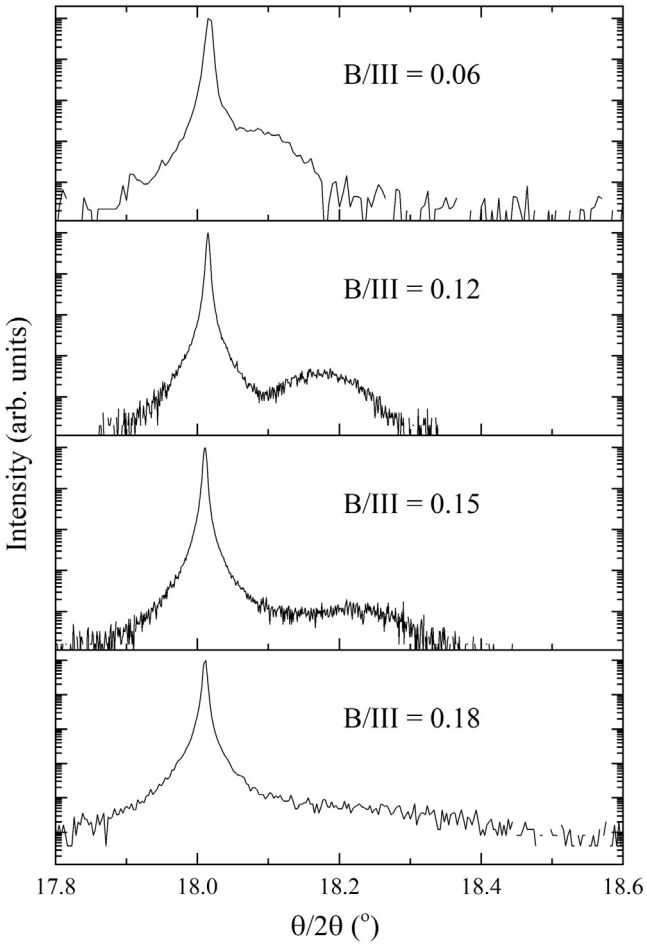

Fig. 2. XRD $\theta/2\theta$ scan of the (0002) plane for the thin films.

function of depth of the scattering atoms. The scattering cross section, which determines the yield, is proportional to Z^2 (Z = atomic number). Therefore, RBS is more sensitive for large atoms, and has a lower detectability for smaller atoms like boron. RBS is also sensitive to the thin film morphology, and thus the columnar growth in our materials provides a challenge [15]. The sum of these issues makes for a large uncertainty in the composition determination by RBS. An example of our RBS measurements for a BAlN film with B/III gas-flow ratio of 0.18 is in Fig. 3, which shows the RBS data and a simulation (smooth line) using XRUMP software [16]. The Al content, calculated by fitting the step in the data near the Al onset, corresponds to 0.84. The boron content is calculated by taking the difference [B] = 1 – [Al] = 0.16. Here we assume that the drop in Al content is due to B atoms substituting Al atoms, and that there are no interstitial B atoms.

3.2. Evolution of the microstructure of BAlN alloys with increasing B/III gas-flow ratio

Fig. 4 shows a cross-sectional TEM image of the $B_xAl_{1-x}N$ film with B/III gas-flow ratio of 0.06 (x = 0.06 by RBS and 0.023 by XRD). The film exhibits a columnar structure with a lateral dimension of ~10 nm. The inset in Fig. 4 is a fast Fourier transform (FFT) pattern, corresponding to the region in the TEM image indicated by a box, and shows only a wurtzite structure. The BAlN film in Fig. 5 grown with a B/III gas-flow ratio of 0.12 (x = 0.11 by RBS and 0.059 by XRD), shows irregular domain boundaries, without noticeable change in the crystal orientation and structure in the FFT pattern (inset).

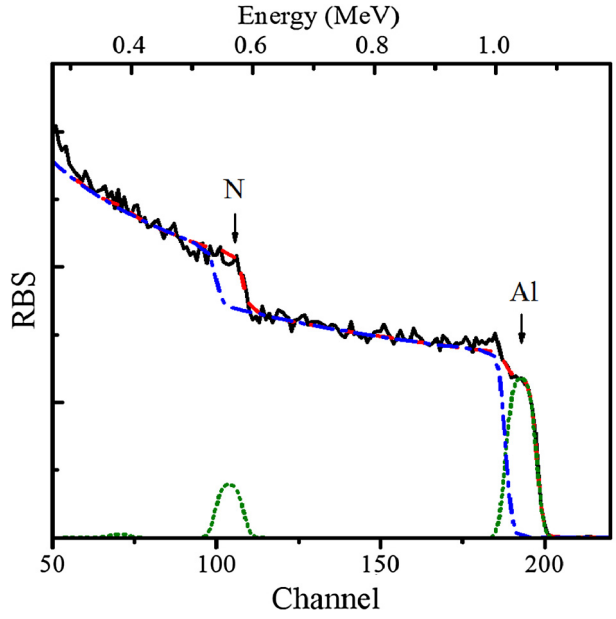

Fig. 3. RBS spectrum for the thin film with B/III = 0.18. The green dotted line and the blue dash-dotted line are the simulations for the BAlN layer and AlN template, respectively. The red dashed line is the sum of the two layers.

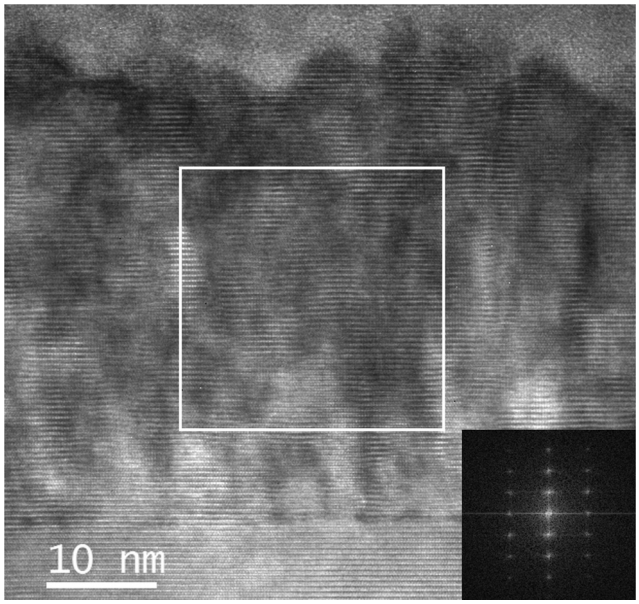

Fig. 4. Microstructure of the BAlN/AlN film grown with a B/III gas-flow ratio of 0.06. Cross-section on-axis multi-beam TEM image along the [1 1 $\bar{2}$ 0] AlN projection. The film is ~45 nm thick and presents a rough surface corresponding to a columnar structure with columns of 10 nm diameter. FFT diffraction pattern of the region in the box indicates the sole presence of a wurtzite structure.

As the boron content is further increased, twin formation is observed in Fig. 6(a) for films grown with a B/III gas-flow ratio of 0.15 (x = 0.14 by RBS and 0.064 by XRD). The bottom region, depicted by the lower box, shows good epitaxy with the *c*-plane parallel to the substrate, as evidenced by the FFT in Fig. 6(b). The FFT pattern in Fig. 6(c), corresponding to the upper box in the TEM image, shows two overlapping crystal structures that result from a twin formation. The extra lattice planes seen in the upper box are (0002) planes tilted by ~60°.

The BAlN film with B/III gas-flow ratio of 0.18 (x = 0.16 by RBS and 0.093 by XRD), shown in the TEM image in Fig. 7(a), exhibits a higher number of twin boundaries than in films with B/III

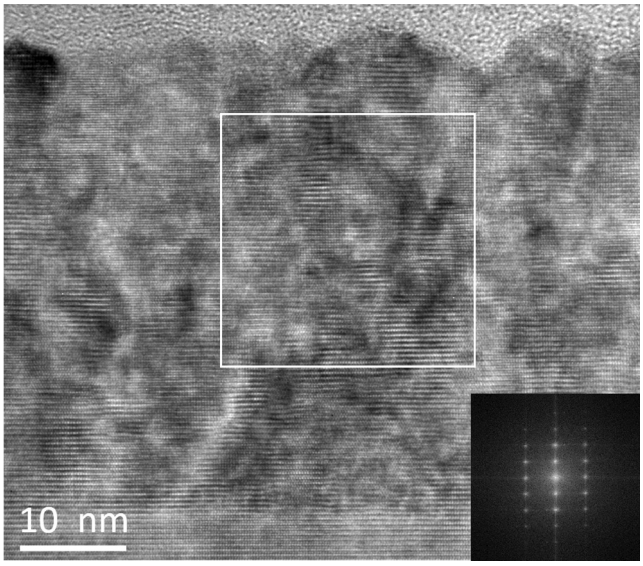

Fig. 5. Microstructure of BAlN film grown with a B/III gas-flow ratio of 0.12. Cross-section on-axis multi-beam TEM image along the [1 1 $\bar{2}$ 0] AlN projection. The film thickness is ~45 nm. FFT diffraction pattern of the region in the box indicating a wurtzite structure.

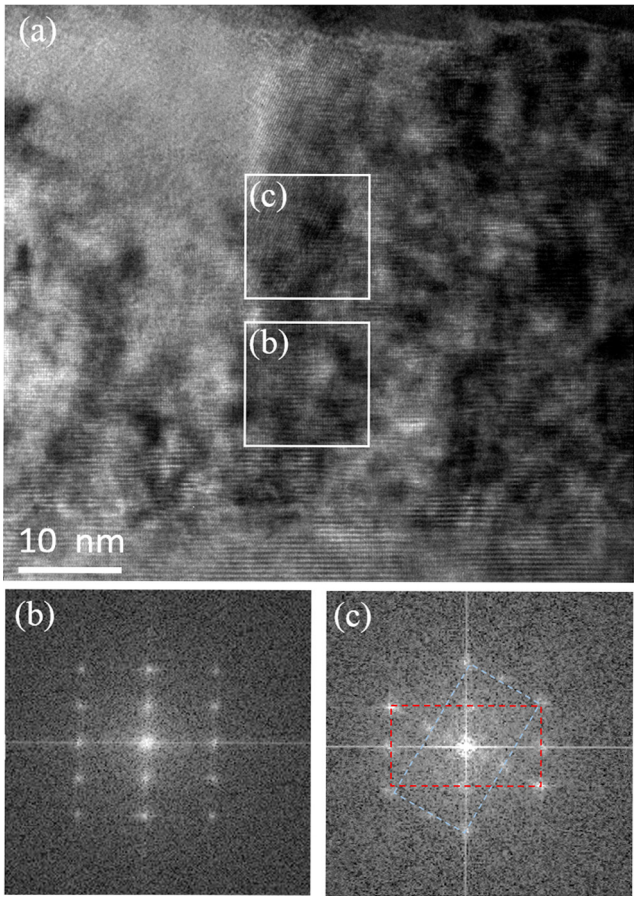

Fig. 6. Microstructure of BAlN/AlN film grown with a B/III gas-flow ratio of 0.15. (a) Cross-section on-axis multi-beam TEM image along the [1 1 $\bar{2}$ 0] AlN projection. The film thickness is ~45 nm. FFT diffraction patterns of the region in the boxes indicate (b) bulk wurtzite BAlN and (c) wurtzite structure rotated ~60°.

gas-flow ratios < 0.15. The region labeled (b) in the image has the same orientation as the AlN underlayer, labeled (c) as observed in the respective FFT patterns in Fig. 7(b) and (c). In a similar manner, the region labeled (d) contains two twin boundaries tilted by ~60°, one clockwise and other counter-clockwise, with respect to the region parallel to the substrate, also included in the FFT pattern. Fig. 7(e) shows the diffraction pattern of a region corresponding to a single twin, rotated clockwise.

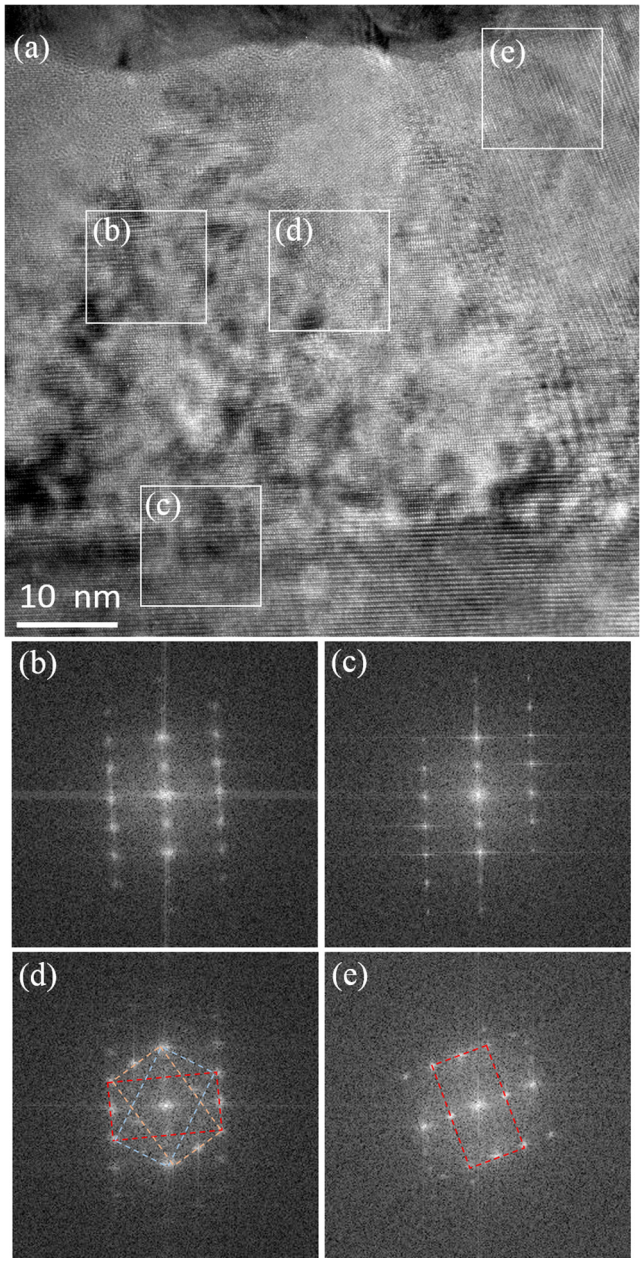

Fig. 7. Microstructure of BAlN/AlN film grown with a B/III gas-flow ratio of 0.18. (a) Cross-section on-axis multi-beam TEM image along the [1 1 $\bar{2}$ 0] AlN projection. (b) FFT diffraction pattern of the BAlN structure with the same orientation as (c) AlN substrate. (d) and (e) FFT diffraction patterns showing twins.

3.3. Twin formation

For B/III gas-flow ratios ≥0.15 (Figs. 6(c) and 7(d) and (e)), we observe the formation of twins. They are observed as extra spots in the diffraction patterns that result from a mirror reflection about certain lattice planes. The relationship between the [1 1 $\bar{2}$ 0] reciprocal lattice projection and two possible twin planes is shown in Fig. 8, corresponding to reflections about {1 $\bar{1}$ 0 1} and {1 $\bar{1}$ 0 3} lattice planes in real space. Enlarged versions of Figs. 7(d) and 6(c) are shown for

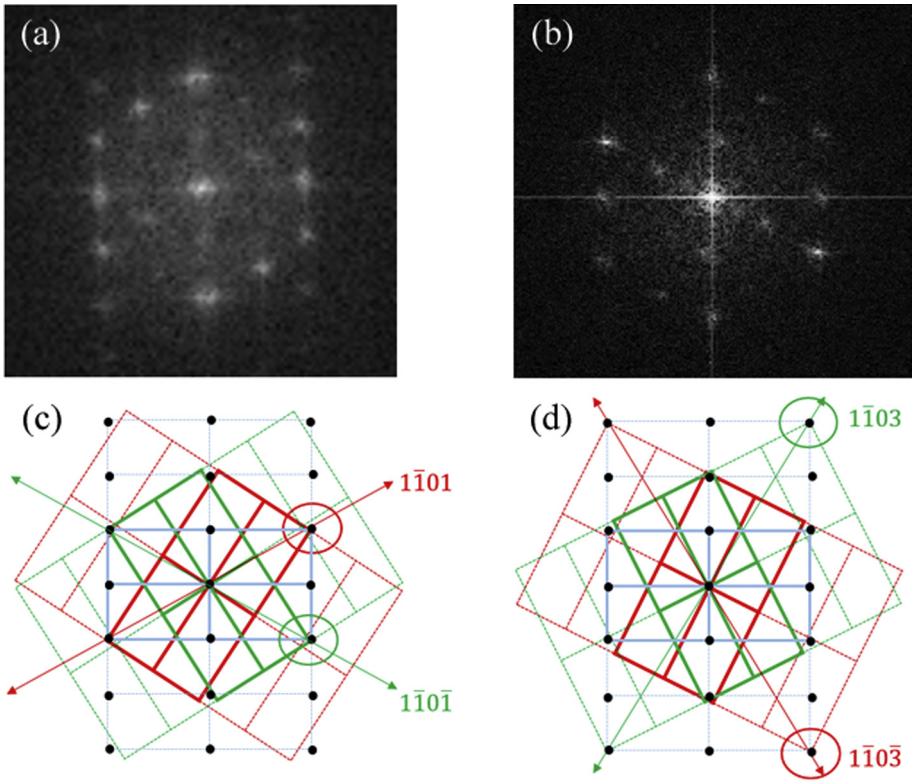

Fig. 8. Diffraction patterns corresponding to twinning in BAlN thin films with B/III gas-flow ratio of (a) 0.18 and (b) 0.15. Schematic diffraction pattern of the twinned BAlN (red and green) and the bulk material (blue) for twinning about (c) $\{1\bar{1}01\}$ and (d) $\{1\bar{1}03\}$ lattice planes in real space. The two diagrams are too similar for accurate experimental identification in the present work. (For interpretation of the references to colour in this figure legend, the reader is referred to the web version of this article.)

comparison with diagrams of the projection of the reciprocal lattice and its twins. Both twinning systems give similar patterns, so we cannot distinguish them from our diffraction patterns. Similar twinning structures have been reported for wurtzite GaN nanostructures [17,18]. It has been reported that the $\{1\bar{1}03\}$ twin planes are energetically preferred in nanowires [19], but we cannot eliminate the possibility of $\{1\bar{1}01\}$ twin planes in our BAlN thin films.

It is important to note that twinned regions in the film will not contribute to the XRD intensity in $\theta/2\theta$ scans, since their basal planes will not be parallel to the substrate.

3.4. Spatial composition variations

The spatial composition variation has been probed using EELS in the TEM. The spectral regions corresponding to the Al *L*-edge, B *K*-edge, and N *K*-edge with the background removed for our film with B/III gas-flow ratio of 0.18 is shown in Fig. 9. The spectra of Al and N closely follow those for slightly oxidized AlN [20]. The uniform spatial distribution of N in Fig. 9(c) indicates a uniform thickness (and density) of the TEM foil. By comparing the concentration of Al and B in Fig. 9(d) and (e), we observe that the two elements have complementary distribution, especially in the encircled region. Only the epitaxial portion outside this region in Fig. 9(e), which has less boron, is expected to contribute to the B content measured by XRD.

4. Discussion

4.1. Absence of phase separation in BAlN alloys

The boron solubility was predicted from the interaction parameter to be x = 0.028 for $B_xAl_{1-x}N$ and y = 0.018 for $B_yGa_{1-y}N$ [9]. In this study, relatively sharp XRD peaks (Fig. 2) were observed corresponding to a boron content up to x = 0.059, and broader peaks were observed indicating boron contents up to x = 0.093 (Fig. 1). As described in a previous section, these boron content values correspond to regions of the film with basal planes parallel to the AlN underlayer, and therefore are evidence of uniform boron incorporation on the planes parallel to AlN. We have looked at other regions of the XRD spectra for evidence of regions of higher boron content, which would result from phase separation, but failed to obtain such evidence. We therefore believe that for our growth technique there is no phase separation of the spinodal type.

The crystal defect structures of our thin films present interesting characteristics. Analysis of the TEM images show the presence of the wurtzite structure throughout all regions studied – we have observed no other phases in electron diffraction patterns. Stacking faults and other disorders in the stacking sequence are not observed, as their presence would result in streaks along the *c*-direction in the FFT patterns. No phase separation is observed in our BAlN/AlN layers. We attribute this to the fact that B atoms are smaller than Al, giving rise to local tensile stress. InGaN alloys are different in that In is larger than Ga, causing compressive strain in InGaN/GaN, with predicted spinodal decomposition [21]. However, under strain-relaxed conditions, high-indium-content InGaN epilayers have been reported without evidence of spinodal decomposition [22].

4.2. Epitaxial growth vs boron incorporation in BAlN alloys

As mentioned above, the proportion of epitaxial growth parallel to the substrate appears to increase linearly with B/III gas-flow ratio, up to a maximum boron concentration of x = 0.093 measured by XRD in this work. On the other hand, RBS measurements suggest that the efficiency of boron incorporation appears to closely follow the gas-flow ratio up a maximum boron concentration of

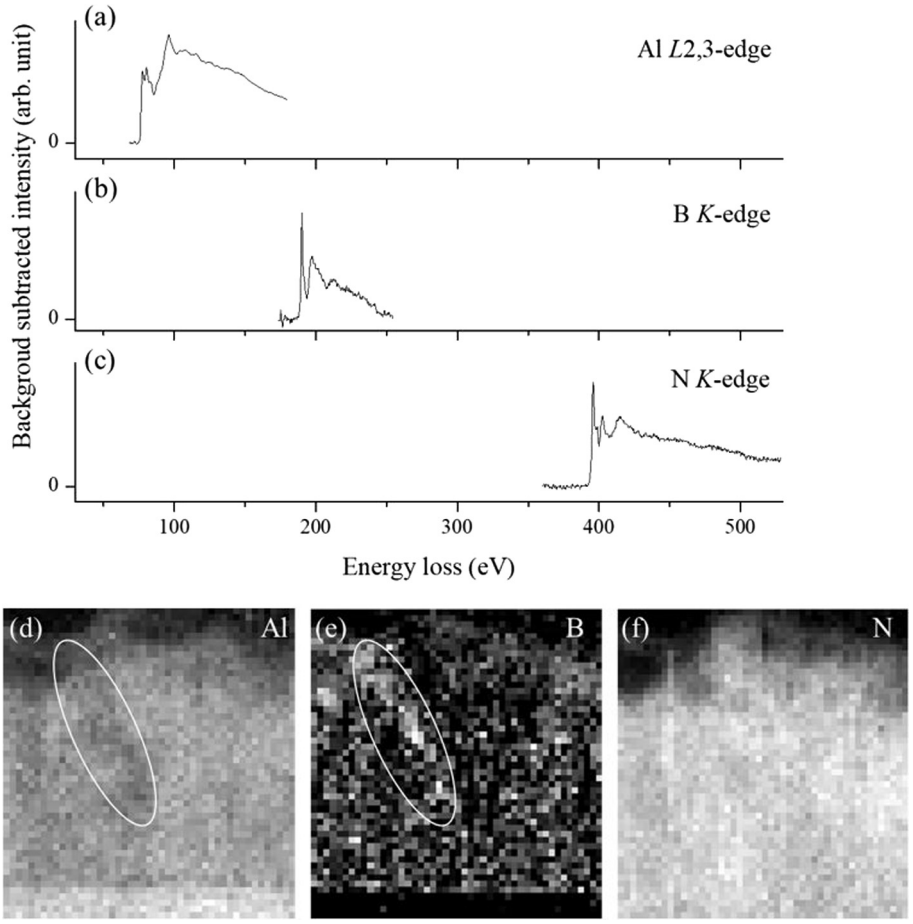

Fig. 9. EELS spectra showing the (a) Al *L*-edge, (b) B *K*-edge, and (c) N *K*-edge after background subtraction, and (d–f) the corresponding compositional mapping of these elements. The circle shows a region of relatively higher boron and lower aluminum content.

$x \approx 0.16$. Following the discussion above, the difference in the boron concentration by XRD and RBS can be explained based on the nature of the measurements. XRD is providing information about regions of parallel epitaxy, while RBS is about the average concentration based on measurement of Al backscattering and III-N stoichiometric considerations. The fact that $\theta/2\theta$ XRD scans do not provide information about regions with basal planes with a non-parallel orientation to the substrate, suggests that those regions may contain the excess boron suggested by the RBS data. Those regions consist of intergranular regions and twins. The spatial compositional variations in Fig. 9 suggest boron segregation at the columnar boundaries. Attempts to accurately measure the composition by EELS have not been successful because of the small probe volumes and the lack of standards for EELS regarding B in BAlN.

4.3. Growth mechanisms and microstructure

The columnar microstructure in Figs. 4 and 5 suggest that the early stages of thin film growth involve island formation of the Volmer-Weber or Stranski-Krastanov types. Tendency towards island formation in the early stages of growth of nitride semiconductors has been reported in the literature for epitaxial growth of GaN on sapphire and on AlN [23,24], and for $B_xGa_{1-x}N$ on GaN and on AlN [2]. Columnar growth has been reported for $B_xAl_{1-x}N$ thin films grown by FME-MOCVD with $x \sim 0.015$ [10], and more recently with $x = 0.12$ [11,13]. We therefore speculate from our TEM observations that for low boron content, well-defined and stable columns result from island growth in the early stages of epitaxy. The surface roughness is related to the columnar lateral dimensions. This is observed in Fig. 4, for growth with B/III gas-flow ratio = 0.06, where the columnar diameter (~10 nm) is similar to the surface roughness period. For higher boron contents, the columnar diameters tend to be smaller, and the columns are not always normal to the substrate. The lattice planes appear to follow the orientation of the substrate even when the columns are inclined. The finer columns tend to coalesce and form smoother growth fronts, as observed in Fig. 5 (for B/III gas-flow ratio = 0.12). The dark regions in the TEM images are attributed to strong diffraction from regions with good alignment of the crystal zone axis with respect to the electron beam. The FFT patterns displayed as insets in the TEM images indicate that the *c*-axis of the columnar structure aligns well with the growth direction, i.e. it is a well-aligned epitaxial film.

5. Summary and conclusions

We have analyzed the microstructure and composition of thick BAlN films with B/III gas-flow ratios ranging from 0.06 to 0.18. For low boron contents, a columnar structure reflects island formation in the early stages of growth. The columnar diameter decreases with boron content. No tilt in the orientation of the columns was observed from diffraction patterns. Twinned regions are observed at B/III gas flow ratios at and above 0.15, ~10 nm in diameter. The B content obtained by RBS closely follows the B/III gas-flow ratio, indicating high efficiency of boron incorporated into the film.

The B content measured by XRD is noticeably less than measured by RBS. Given that $\theta/2\theta$ XRD spectra are sensitive only to crystal regions that are parallel to the substrate, and in the absence of tilted regions, we attribute this difference to possible boron segregation at the columnar boundaries and other crystalline defects such as twinned regions. We have observed no evidence of phase separation in our films.

Acknowledgements

This work was supported by the U.S. National Science Foundation under DMR-1410874. XHL acknowledges support of the KAUST startup and baseline funding. RDD acknowledges support of the Steve W. Chaddick Endowed Chair in Electro-Optics and the Georgia Research Alliance. The authors acknowledge beneficial discussion of RBS data with Daniel Tseng from Evans Analytical Group, and Dr. Barry Wilkens from Arizona State University. The authors acknowledge the help in EELS from Jing Lu and Dr. Ray Carpenter from Arizona State University.

References

[1] A. Ougazzaden, S. Gautier, C. Sartel, N. Maloufi, J. Martin, F. Jomard, J. Cryst. Growth 298 (2007) 316.
[2] T. Akasaka, Y. Kobayashi, T. Makimoto, J. Cryst. Growth 298 (2007) 320.
[3] M. Abid, T. Moudakir, G. Orsal, S. Gautier, A. En Naciri, Z. Djebbour, J.H. Ryou, G. Patriarche, L. Largeau, H.J. Kim, Z. Lochner, K. Pantzas, D. Alamarguy, F. Jomard, R.D. Dupuis, J.P. Salvestrini, P.L. Voss, A. Ougazzaden, Appl. Phys. Lett. 100 (2012) 1.
[4] V. Ravindran, M. Boucherit, A. Soltani, S. Gautier, T. Moudakir, Appl. Phys. Lett. 100 (2012) 243503.
[5] V. Vezin, S. Yatagai, H. Shiraki, S. Uda, Jpn. J. Appl. Phys. 36 (1997) L1483.
[6] A.Y. Polyakov, M. Shin, M. Skowronski, D.W. Greve, R.G. Wilson, A.V. Govorkov, R.M. Desrosiers, J. Electron. Mater. 26 (1997) 237.
[7] C.H. Wei, Z.Y. Xie, J.H. Edgar, K.C. Zeng, J.Y. Lin, H.X. Jiang, C. Ignatiev, J. Chaudhuri, D.N. Braski, MRS Proc. 537 (1998) G3.79.
[8] G. Orsal, N. Maloufi, S. Gautier, M. Alnot, A.A. Sirenko, M. Bouchaour, A. Ougazzaden, J. Cryst. Growth 310 (2008) 5058.
[9] C.H. Wei, J.H. Edgar, J. Cryst. Growth 208 (2000) 179.
[10] T. Akasaka, T. Makimoto, Appl. Phys. Lett. 88 (2006) 1.
[11] X. Li, S. Sundaram, Y. El Gmili, T. Moudakir, F. Genty, S. Bouchoule, G. Patriarche, R.D. Dupuis, P.L. Voss, J.P. Salvestrini, A. Ougazzaden, Phys. Status Solidi Appl. Mater. Sci. 212 (2015) 745.
[12] N. Kobayashi, T. Makimoto, Y. Yamauchi, Y. Horikoshi, J. Appl. Phys. 66 (1989) 640.
[13] X. Li, S. Wang, H. Liu, F.A. Ponce, T. Detchprohm, R.D. Dupuis, Phys. Status Solidi 1600699 (2017), doi: 10.1002/pssb.201600699.
[14] V.L. Solozhenko, D. Häusermann, M. Mezouar, M. Kunz, Appl. Phys. Lett. 72 (1998) 1691.
[15] N.P. Barradas, C. García Núñez, A. Redondo-Cubero, G. Shen, P. Kung, J.L. Pau, Nucl. Instrum. Meth. Phys. Res. Sect. B Beam Interact. Mater. Atoms. 371 (2016) 116.
[16] L.R. Doolittle, Nucl. Inst. Meth. Phys. Res. B 9 (1985) 344.
[17] S. Dai, J. Zhao, M.R. He, H. Wu, L. Xie, J. Zhu, J. Phys. Chem. C 117 (2013) 12895.
[18] Z. Chen, C. Cao, H. Zhu, Chem. Vap. Depos. 13 (2007) 527.
[19] A. Béré, A. Serra, Phys. Rev. B 68 (2003) 1.
[20] V. Serin, C. Colliex, R. Brydson, S. Matar, F. Boucher, Phys. Rev. B 58 (1998) 5106.
[21] I. Ho, G. Stringfellow, Appl. Phys. Lett. 69 (1996) 2701.
[22] A.M. Fischer, Y.O. Wei, F.A. Ponce, M. Moseley, B. Gunning, W.A. Doolittle, Appl. Phys. Lett. 103 (2013) 1.
[23] H. Fujii, C. Kisielowski, J. Krueger, M.S.H. Leung, R. Klockenbrink, M. Rubin, E.R. Weber, MRS Proc. 449 (1996) 227.
[24] B. Daudin, F. Widmann, G. Feuillet, Y. Samson, M. Arlery, J.L. Rouviere, Phys. Rev. B 56 (1997) 7069.